SANDIA REPORT

SAND2013-2664
Unlimited Release
Printed April 2013

Time-Resolved Broadband Cavity-Enhanced Absorption Spectroscopy for Chemical Kinetics

Leonid Sheps, David W. Chandler

Prepared by
Sandia National Laboratories
Albuquerque, New Mexico 87185 and Livermore, California 94550

Sandia National Laboratories is a multi-program laboratory managed and operated by Sandia Corporation, a wholly owned subsidiary of Lockheed Martin Corporation, for the U.S. Department of Energy's National Nuclear Security Administration under contract DE-AC04-94AL85000.

Issued by Sandia National Laboratories, operated for the United States Department of Energy by Sandia Corporation.

Available to DOE and DOE contractors from
U.S. Department of Energy
Office of Scientific and Technical Information
P.O. Box 62
Oak Ridge, TN 37831

Telephone: (865) 576-8401
Facsimile: (865) 576-5728
E-Mail: reports@adonis.osti.gov
Online ordering: http://www.osti.gov/bridge

Available to the public from
U.S. Department of Commerce
National Technical Information Service
5285 Port Royal Rd.
Springfield, VA 22161

Telephone: (800) 553-6847
Facsimile: (703) 605-6900
E-Mail: orders@ntis.fedworld.gov
Online order: http://www.ntis.gov/help/ordermethods.asp?loc=7-4-0#online

SAND2013-2664
Unlimited Release
Printed April 2013

Time-Resolved Broadband Cavity-Enhanced Absorption Spectroscopy for Chemical Kinetics

Leonid Sheps, David Chandler
Combustion Chemistry and Diagnostics Department
Sandia National Laboratories
P.O. Box 969, MS 9055
Livermore, California, 94551

Abstract

Experimental measurements of elementary reaction rate coefficients and product branching ratios are essential to our understanding of many fundamentally important processes in Combustion Chemistry. However, such measurements are often impossible because of a lack of adequate detection techniques. Some of the largest gaps in our knowledge concern some of the most important radical species, because their short lifetimes and low steady-state concentrations make them particularly difficult to detect. To address this challenge, we propose a novel general detection method for gas-phase chemical kinetics: time-resolved broadband cavity-enhanced absorption spectroscopy (TR-BB-CEAS). This all-optical, non-intrusive, multiplexed method enables sensitive direct probing of transient reaction intermediates in a simple, inexpensive, and robust experimental package.

ACKNOWLEDGMENTS

We thank Dr. David Osborn (8353) and Dr. Steven S. Brown (NOAA, Boulder, CO) for helpful discussions regarding cavity-enhanced optical methods and experimental design. We also thank Dr. Craig Taatjes (8353) for the use of lab space and for the loan of a YAG laser and optics.

CONTENTS

FIGURES

NOMENCLATURE

CCD	Charge-Coupled Device
CEAS	Cavity-Enhanced Absorption Spectroscopy
L_{eff}	Effective Path Length
OD	Optical Density
R	Reflectivity
Re	Reynolds Number
SNL	Sandia National Laboratories
TTL	Transistor-Transistor Logic
YAG	Yttrium Aluminum Garnet

1. INTRODUCTION

Many of today's emerging engine technologies rely on accurate understanding of fuel chemistry for increasing efficiency, reducing pollutant emissions, and finding alternatives to fossil-based fuels. Predictive modeling of modern engine performance requires the use of extensive kinetic mechanisms, which in turn depend on a detailed knowledge of gash-phase chemical kinetics. The inherent complexity of this problem demands a hybrid approach that employs computational chemistry tools along with experimental determination of gas-phase reaction parameters, such as elementary rate coefficients and product branching yields.

However, such experimental measurements are often impossible because of a lack of adequate probe methods. Direct detection is particularly difficult for many reactive intermediates (such as radical species) because of their short lifetimes and low steady-state concentrations. The problem is often exacerbated by secondary radical-radical chemistry and by heterogeneous reactions that occur on reactor walls or sampling probes inserted in the reaction mixture. To address these challenges, the ideal experimental detection technique must meet the following requirements:

i. *Non-intrusive probing of the reaction zone:* Homogeneity of the sample is crucial to reliable measurements of elementary reaction kinetics. In order to prevent signal degradation associated with physical probes used to sample out of the reactor, we wish to probe only homogeneous regions away from all surfaces and to not disturb the reactive mixture.

ii. *Multiplexed detection:* Simultaneous probing of multiple chemical species reduces systematic errors in measuring branching fractions and enables unambiguous kinetic assignments, e.g. of sequential reaction pathways, A → B → C.

iii. *Direct time-resolved probing:* Direct measurement of species time-histories is the simplest way to determine reaction rate coefficients. Ideally, transient populations of reactants must be prepared near-instantaneously with a photolysis laser pulse, and their evolution monitored in real time with <10 μs resolution.

iv. *High sensitivity:* Radical-radical reactions are frequently very fast, with rate coefficients that approach gas-kinetic values (~$1\cdot10^{-10}$cm^{3}molec^{-1}s^{-1}). In order to avoid secondary chemistry, reacting samples have to be very dilute (initial radical concentrations << 10^{14}cm^{-3}), which calls for a sensitive probe method.

Some of the experimental detection methods currently in wide use in gas-phase chemical kinetics include conventional absorption spectroscopy, laser-induced fluorescence, gas chromatography, and photoionization mass spectrometry. These methods excel at one or more of the above requirements, but do not meet all of them simultaneously. The purpose of this LDRD project is to develop a novel optical absorption technique that does fulfill all four requirements and enables efficient kinetic measurements in a simple and inexpensive experimental package. Optical absorption, commonly expressed as optical density (OD), is given by the Beer-Lambert Law:

$$OD = -\ln\frac{I}{I_0} = \sigma \cdot C \cdot l \qquad \text{eq. (1)}$$

where I and I_0 are probe radiation intensity with and without the absorbing species, respectively, σ is the absorption cross-section, C is the species concentration, and l is the sample path length. Since the radical concentration C must be kept low, we will use cavity-enhanced absorption methods to maximize effective path lengths (L_{eff}) for increased sensitivity.

2. EXPERIMENTAL STRATEGY

Figure 1 is a cartoon of the overall experimental design: time-resolved broadband cavity-enhanced absorption spectroscopy (TR-BB-CEAS). The proposed technique rests on three main components. The first is a broadband resonator cavity, capable of achieving long effective path lengths over the entire visible wavelength range (370 – 700 nm). The increase in L_{eff} results from the probe radiation being "trapped" for multiple passes inside the resonator cavity and in turn yields an equivalent increase in measured transient absorption. The second component is a slow-flow reactor that allows photolytic initiation of gas-phase chemical reactions in a homogeneous environment with well-defined conditions: temperature, pressure, and mixture composition. The reactor is integrated into the optical resonator cavity for real-time transient absorption probing of the reaction progress. The final experimental component is a novel spectrometer, designed to disperse the cavity output in wavelength and time domains and to record the entire absorption spectrum as a function of kinetic time. The three components are described in detail in the following sections.

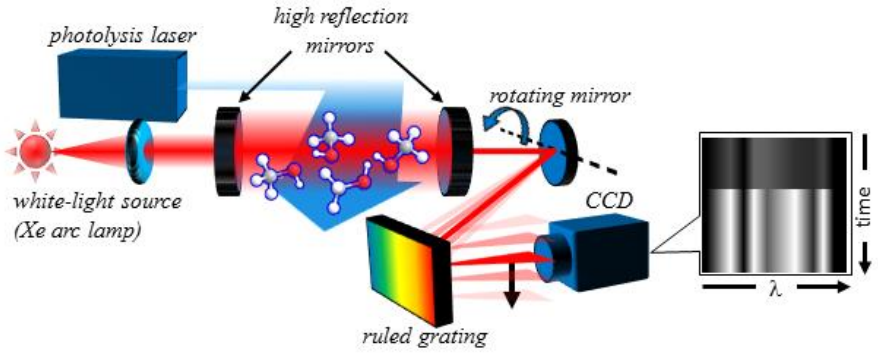

Figure 1. TR-BB-CEAS experimental setup.
The TR-BB-CEAS setup includes a white-light probe source, a broadband optical cavity integrated with a photolytic-initiation chemical reactor, and a time-resolved spectrometer.

2.1 Broadband Optical Resonator

2.1.1 Principles of Cavity-Enhanced Methods

A detailed analysis of optical resonators is beyond the scope of this report, and several excellent reviews are available in the literature [1-4]. Nonetheless, some key concepts can be summarized by a few simple rules. Consider a cavity consisting of two highly reflective mirrors with identical reflectivity R (where R approaches 1) separated by a distance D, and no other appreciable losses.

- If this cavity is exposed to radiation from a pulsed laser (pulse duration much shorter than the round-trip time in the cavity), a small fraction of the incoming light transmits through the input mirror and resonates in the cavity with a small loss through the output mirror on each round trip. The cavity output will be an exponentially decaying series of pulses with 1/e decay time τ [1, 2]:

$$\tau = \frac{D}{c \cdot |\ln(R)|} \simeq \frac{D}{c \cdot (1-R)} \qquad \text{eq. (2)}$$

The decay time represents average photon lifetime in the resonator, and equation (2) can be rearranged to yield the effective path length in the cavity: $L_{eff} = D \cdot (1-R)^{-1}$. For example, R=99% cavity mirrors result in about 100 passes, or 50 round trips.

- In the case of continuous input light, such a cavity is resonant with any radiation with frequency $\nu = q \cdot c/2D$, where q is an integer and c is the speed of light. Since multiple frequencies fulfill this relationship, they form a series of resonant *axial frequency modes*, each with a bandwidth $\Delta\nu$:

$$\Delta\nu \simeq \frac{c}{2D} \cdot \frac{1-R^2}{\pi \cdot R} \qquad \text{eq. (3)}$$

Broadly speaking, input radiation that falls under the bandwidth of one of these modes enters the cavity and resonates within it, otherwise, the radiation is reflected back [3, 5]. In analogy to the pulsed input light, resonant continuous radiation builds up in the cavity to a circulating intensity

$$I_{circ} \simeq I_{in} \cdot \frac{1}{1-R} \qquad \text{eq. (4)}$$

The input and output transmissions are continuous, and the steady-state intensity buildup in the cavity is a measure of the average photon lifetime and thus the effective path length inside the resonator. Once again, 99% reflective mirrors yield about 100 trips inside the resonator. Higher mirror reflectivity results in longer effective path lengths but also narrower resonant modes.

Typical cavity-enhanced absorption techniques employ very highly reflective mirrors (up to R = 99.9999%), which in principle yields very long L_{eff} and excellent detection sensitivities [6, 7]. To achieve their full potential, such experiments must actively lock the probe laser frequency to the cavity and match the source spectral shape and spatial profile to the cavity frequency and spatial modes – a difficult task that requires complex and expensive equipment [8, 9].

In contrast, incoherent broadband cavity-enhanced absorption utilizes simple lamps to provide spectrally broad probe radiation that excites all accessible cavity modes simultaneously [10]. Because the cavity is not stabilized in any way, the center frequencies of the cavity modes rapidly fluctuate, and on average cavity enhancement occurs evenly across the entire wavelength spectrum. Thus, time-averaged resonator output can be used to monitor intra-cavity absorption with a significantly simpler experimental setup at the price of somewhat lower detection sensitivity.

2.1.2 Implementation of Broadband Optical Resonator

Our optical resonator is based on the principles of cavity-enhanced optical methods described above, but with a tenfold increase in spectral range compared with the best existing broadband setups [1]. According to equation (4), small fluctuations in R result in pronounced variations of L_{eff} across the spectrum. Because of this, the main design considerations were to achieve high yet fairly constant mirror reflectivity over a maximum spectral range. Our mirrors are manufactured by JDSU, Inc., and specified to have R = 99.4% ± 0.2% from λ = 370 to 700 nm, representing the current state-of-the-art in optical coating technology. The mirrors are plano-concave, with radius of curvature r = 5.000 m, and the cavity length is 1.6 m.

The probe radiation comes from a 75-Watt Xe arc lamp (Newport Corp.), which provides a relatively noise-free, spectrally flat output in the 300 – 2400 nm range. A 50-mm diameter, F/1 UV fused silica lens focuses the lamp output and a Schott Glass KG2 filter restricts the probe spectrum to the 370 – 750 nm wavelength range. Figure 2 shows the measured cavity output spectrum (upper panel). The output is a convolution of the input spectrum with the cavity buildup spectrum, which is in turn determined by the mirror reflectivity curve (lower panel in Figure 2). Since this is a low-finesse cavity with an incoherent light source, L_{eff} cannot be reliably calculated and must be independently measured (see below).

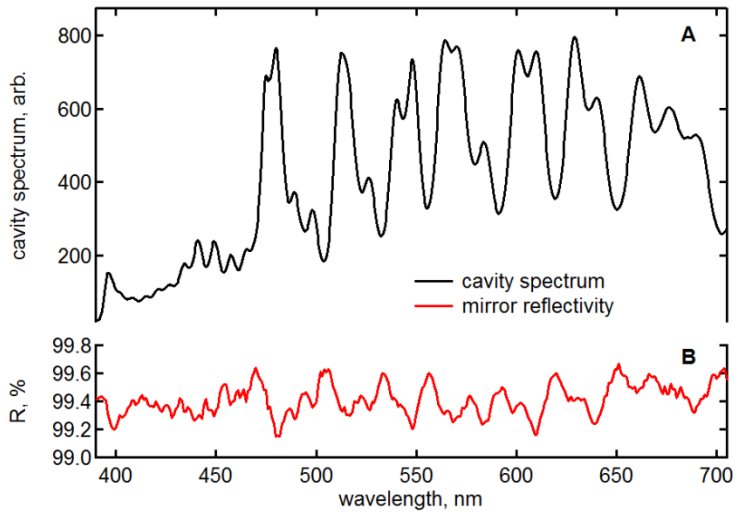

Figure 2. Broadband resonator spectrum
Panel A: Experimentally measured cavity output spectrum with a Xe arc lamp as a probe radiation source. *Panel B*: Cavity mirror reflectivity curve supplied by the manufacturer.

2.2 Slow-Flow Chemical Reactor

The chemical reactor is a 120-cm long quartz tube with an internal diameter of 3 cm. The tube contains several ⅛-inch inner diameter (ID) quartz side arms that can be used as gas inlets or as thermocouple access points for temperature measurements inside the reactor. Calibrated mass flow controllers (MKS Instruments) supply the gaseous sample components, which mix before entering the reaction cell. A roots blower pumps the reactor through a ½-inch ID pump port. An active feedback-controlled butterfly valve positioned downstream maintains the desired reactor pressure, measured by capacitance manometer (MKS Instruments).

The quartz cell is positioned between two heavy stainless steel support towers that minimize mechanical vibrations of the reactor and resonator cavity. The towers also house the highly reflective end mirrors that form the optical resonator cavity and the uncoated windows (UV Fused Silica) that admit the photolysis laser pulse. The cavity mirrors are held in kinematic adjustable mounts, coupled to the reactor by flexible steel bellows, which allows for resonator alignment while under vacuum. Precise knowledge of the probe volume geometry is critical to obtaining quantitative absorption measurements, and therefore we take special care to define the pump-probe overlap volume. The photolysis laser pulse, provided by either an excimer or a YAG laser, is expanded by a 4:1 telescope and apertured down with an iris, giving a 20-mm diameter

spot with a nearly flat "top hat" intensity profile. The angle between the pump (photolysis) and probe (resonator cavity) beams is 2º, which yields an 80-cm long homogeneous excitation profile.

The reactor is designed to operate at sample pressures of up to 1 atm. A key consideration for cavity-enhanced absorption measurements is the need to avoid sample turbulence, which interferes with the optical resonator performance. In general, turbulence depends on gas mixture composition, pressure, and flow speed; therefore, gas flow in the reactor should be large enough to replenish the sample between successive photolysis laser shots, yet small enough to keep the Reynolds number in the laminar flow regime (Re < 2300). The benchmark experiments described in this report were performed using N_2 as a carrier gas at pressures of 1 – 10 torr and sample speeds of 1 – 2 m/s, corresponding to Re ≤ 50. At 1 atm, the sample flow speed is limited to ~1 m/s (Re ~2000 at room temperature).

In addition, the reactor can withstand temperatures up to 1000 K. The heating system, to be constructed in the near future, will include a tubular ceramic fiber heater jacket and a feedback-controlled current supply.

2.3 Time-Resolved Absorption Spectrometer

The transient spectrum of the reacting gas mixture is recorded by a homebuilt time-resolved spectrometer, based on the principle of "spectral photography" proposed by Scherer *et al*. [11]. A ruled optical grating disperses the probe cavity output in wavelength horizontally and projects it onto a CCD camera. Meanwhile, a spinning mirror sweeps the entire output spectrum vertically across the CCD detector. In this way, spectral and temporal information are mapped spatially onto the camera, creating a two-dimensional "transient absorption image" of a chemical reaction.

The CCD camera (Andor Technology) has a 1024x1024 pixel sensor, approximately 13x13 mm in size. It is cooled by a thermoelectric cooler, which minimizes readout noise as well as dark noise during long integration times. The CCD chip includes a UV-enhanced coating, giving a nearly uniform quantum efficiency of about 0.6 in the 250 – 800 nm spectral range.

The optical grating is positioned 80 mm away from the camera, and its groove density determines the wavelength range that is imaged by the CCD camera in the horizontal direction. A cylindrical focusing lens (UV Fused Silica, F=50mm) ensures a tight wavelength focus at the camera, such that the resolving power of the spectrometer is limited only by the spatial resolution of the CCD chip. A simple replacement of the grating by one with a higher or lower groove density changes the full-scale spectral range and the spectral resolution, if necessary.

The spinning mirror is located 75 mm before the grating and is driven by a phase-locked, feedback-controlled motor. The duration of the sweep across the camera screen is inversely proportional to the mirror rotation frequency: at 10 Hz, the probe spectrum traverses the CCD chip in 1.3 ms (1.3 μs/pixel). A separate cylindrical lens (UV Fused Silica, F=150mm) focuses the probe light in the vertical direction, resulting in a spatial focus on the CCD screen with a width of ~ 8 pixels and a total kinetic time resolution of 10 μs. Better kinetic resolution is available by simply increasing the mirror rotation speed.

Whereas the original "spectral photography" design of Scherer and co-workers was a single-shot method with 30-nm probe bandwidth [11], our spectrometer operates over a 10x greater spectral range and allows for extensive signal averaging by externally synchronizing the photolysis laser

with the mirror motor. An optical sensor in the motor head produces a TTL-level pulse train that triggers the laser. A digital delay generator introduces a variable delay into the laser trigger, thus mapping the photolysis time spatially onto the appropriate position on the CCD screen. The camera operates in the "long exposure" mode, and transient absorption measurements are accumulated directly on the CCD chip over multiple laser shots.

A custom-written LabView program acquires the data and handles simple image processing tasks, such as averaging and background subtraction. We take a series of alternating transient absorption (photolysis laser ON) and reference (laser OFF) images; the transient optical density spectrum is calculated from the ratio of these images according to equation (1).

3. CALIBRATION AND PERFORMANCE OF TR-BB-CEAS METHOD

3.1 Wavelength Calibration

The time-resolved spectrometer was calibrated against a commercial grating-based spectrometer (Thorlabs) using the structured buildup spectrum of the optical resonator itself. The calibration was checked using atomic emission lines from Hg and Ne pencil-style calibration lamps (Oriel). The spectrometer alignment proved to be robust and did not change day-to-day. The spectral resolution and performance was validated using the well-known spectrum of NO_2 [12]. Figure 3 shows the measured absorption of nitrogen dioxide with the resonator cavity operating in single-pass mode, and containing a dilute mixture of 0.5% NO_2 in 25 Torr of N_2. The red trace is the literature absorption cross-section of NO_2 [12], offset vertically for clarity. The black trace is a single-pass absorption spectrum of a gaseous sample of NO_2.The use of a 600 groove/mm optical grating resulted in a ~390-nm full-scale spectral range and a wavelength dispersion of ~0.38 nm/pixel. The measured spectrum agrees very well with the literature values, showing that our spectral resolution is limited only by the spatial resolution of the CCD chip.

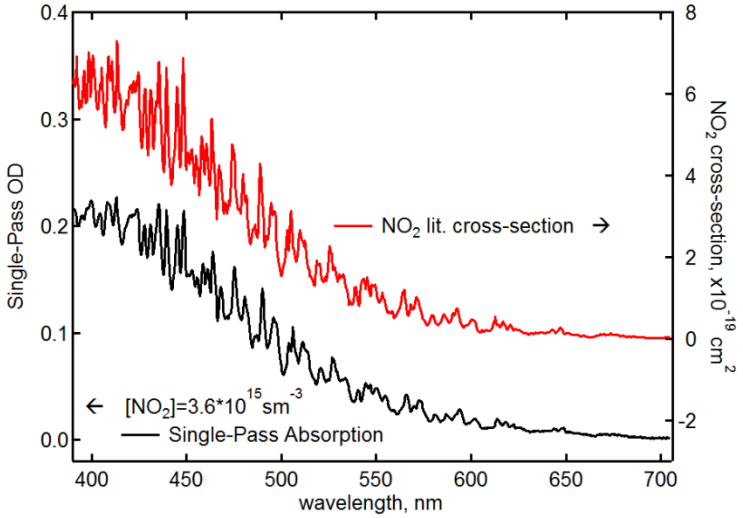

Figure 3. Wavelength calibration of the time-resolved spectrometer.

3.2 Kinetic Time Calibration

The temporal response function of the spectrometer was determined by introducing a variable delay into the photolysis laser trigger relative to the mirror rotation angle, and imaging the laser scatter onto the CCD camera. The photolysis radiation came from the 4th harmonic of a YAG (λ = 266nm), which is not directly imaged by the spectrometer. However, a white card placed in the photolysis path in front of the spectrometer entrance slit produces sufficient blue scatter to illuminate the camera sensor and form a narrow horizontal line, marking the spatial position of the mirror sweep. Figure 4 shows the temporal response measurement for three different mirror rotation frequencies: 2, 5, and 10 Hz. The symbols indicate the position on the CCD screen corresponding to a particular delay; the dotted lines are linear least-squares fits with slopes of

6.54, 2.60, and 1.28 μs/pixel. Kinetic time maps linearly onto CCD pixel position and the full-scale range of accessible kinetic times is easily adjusted to "zoom in" or "zoom out" in time.

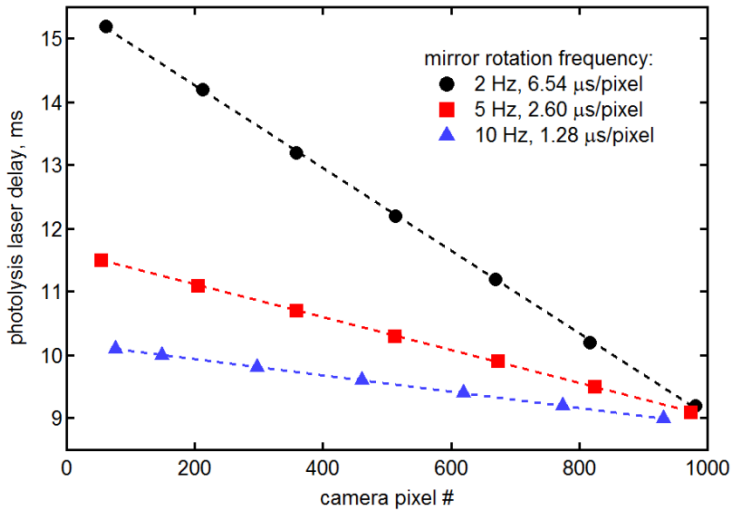

Figure 4. Kinetic time calibration of the TR-BB-CEAS instrument.

3.3 Effective Path Length

Precise knowledge of the effective path length is critical to quantitative measurements of species concentrations by optical absorption. This is trivial in single-pass direct absorption experiments, but is usually much more complicated for cavity-enhanced methods because the exact number of round trips through the cavity is not known *a priori*. In pulsed-laser applications the ringdown time of high-finesse optical cavities can be measured directly; however, for continuous-wave CEAS setups L_{eff} must be determined with a known standard.

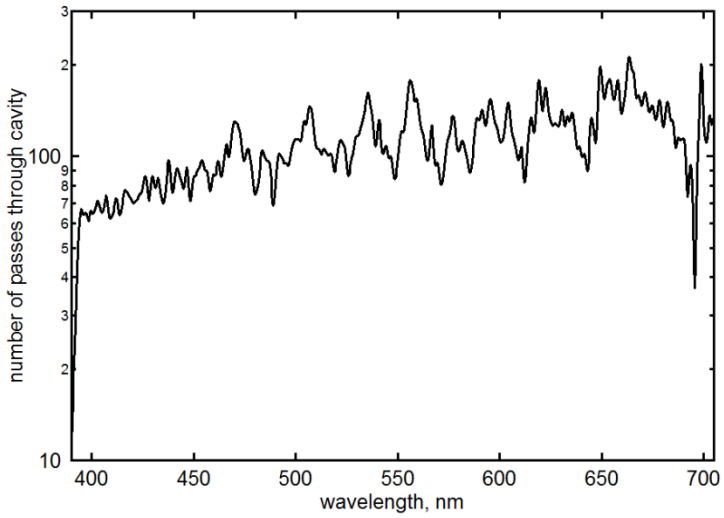

Figure 5. Effective path length determination of the TR-BB-CEAS cavity.

Measurement of the effective path length in our broadband resonator is especially challenging, because L_{eff} depends on the cavity mirror reflectivity, which in turn varies with wavelength. We

calibrate L_{eff} over the entire spectral range at once using a known concentration of NO_2 as a "molecular absorption standard" with a broad spectrum. This calibration method is reliable up to ~650 nm, where NO_2 absorption cross-section diminishes greatly. Future experiments that require accurate knowledge of L_{eff} at longer wavelengths will utilize I_2 as an absorption standard.

Figure 5 shows L_{eff}, expressed as the average number of passes through the cavity, as a function of wavelength. A minor fluctuation of ±0.2% in mirror reflectivity results in noticeable variation of L_{eff} across the visible wavelength range, from ~70 to ~200 passes. Despite this variation, we can use the independent determination of L_{eff} to quantitatively analyze transient measurements. Combined with the knowledge of pump-probe overlap length, the effective path length in photolysis-initiated kinetic experiments is 56 – 160 m, depending on the wavelength. We also note that because our resonator cavity is designed to have low finesse, it is relatively insensitive to alignment; consequently, L_{eff} does not change greatly from day to day.

Figure 6 plots the transient absorption spectrum (averaged between t = 0.1 and t = 0.7 ms) of the photodissociation of isopropyl nitrate ($C_3H_7ONO_2$) at 266 nm. This reaction was recently shown to produce NO_2 with unity yield [13] at the experimental conditions used here (6.5 or 10 Torr, T = 300 K). Using the known initial concentration of isopropyl nitrate, its absorption cross-section at 266 nm, and the photolysis fluence, we expect to detect NO_2 products at concentrations of $2.23 – 3.47 \cdot 10^{12}$ cm^{-3}. The measured concentrations are in superb agreement with the predictions, with differences of less than 3%, showcasing our ability to quantitatively measure chemical species populations. The inset of Figure 6 shows a kinetic trace of NO_2 production, integrated between λ = 420 and 455 nm. The trace shows sharp production of NO_2 within about 10 pixels (0.06 ms), in agreement with the calculated temporal resolution at 2 Hz mirror rotation.

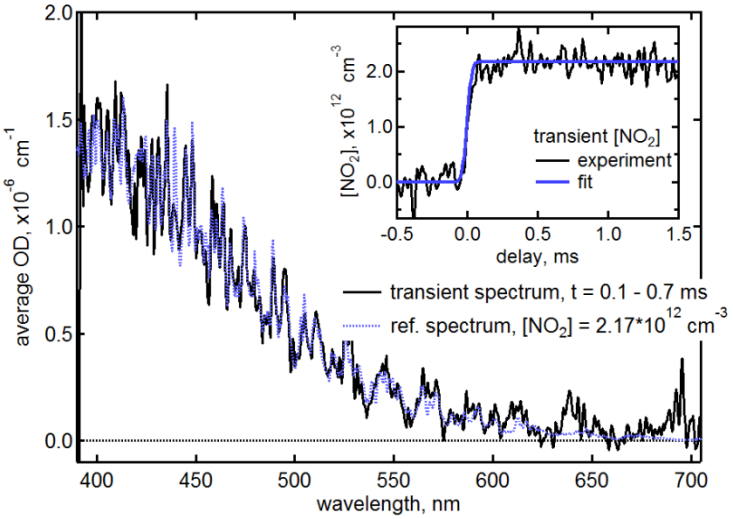

Figure 6. Photolysis of isopropyl nitrate.
Black trace: transient absorption spectrum following photodissociation of isopropyl nitrate at 266 nm. Dotted blue line: reference spectrum of NO_2 with a concentration of $2.17 \cdot 10^{12}$ cm^{-3}. *Inset:* Time trace of NO_2 concentration. Solid blue line is a fit to a step-function rise, convoluted with a Gaussian temporal response function (full width at half-maximum is 10 pixels).

4. STUDIES OF VINYL RADICAL OXIDATION

The first studies of gas-phase chemical kinetics using our newly-developed experimental apparatus focused on vinyl radical oxidation. The reaction of vinyl (C_2H_3) with O_2 is an excellent benchmark chemical system because it is relatively simple and well-understood [14], yet it clearly illustrates many of the advantages of the TR-BB-CEAS technique. The vinyl radical is one of the simplest unsaturated hydrocarbon radicals and is of central importance in combustion and planetary atmospheric processes. It has a well-characterized absorption band in the 400 – 530 nm range (the $A\ ^2A'' \leftarrow X\ ^2A'$ transition) with an extensive vibrational progression and a moderate absorption cross-section (~ $3 \cdot 10^{-19} cm^2$ at 404 nm) [15-17]. In the presence of O_2 the main decay pathways of the vinyl radical are shown below [14, 18]:

$$C_2H_3 + C_2H_3 \rightarrow C_2H_4 + C_2H_2 \qquad k_{1a} = 9.5 \cdot 10^{-11} cm^3 molec^{-1} s^{-1} \quad (1a)$$

$$C_2H_3 + C_2H_3 + M \rightarrow C_4H_6 + M \qquad k_{1b} = 2.5 \cdot 10^{-11} cm^3 molec^{-1} s^{-1} \quad (1b)$$

$$C_2H_3 + O_2 \rightarrow CH_2O + HCO \qquad k_2 = 1 \cdot 10^{-11} cm^3 molec^{-1} s^{-1} \quad (2)$$

The self-reaction pathways (1a) and (1b) are disproportionation and combination, respectively. It should be noted that reaction (1b) is a three-body process, mediated by collisions with bath gas molecules M, and the rate coefficient k_{1b} listed above is a high-pressure limit value. Pathway (2) is the oxidation reaction that forms solely formaldehyde and HCO, the formyl radical. HCO, in turn, reacts with molecular oxygen [19]:

$$HCO + O_2 \rightarrow CO + HO_2 \qquad k_3 = 5 \cdot 10^{-12} cm^3 molec^{-1} s^{-1} \quad (3)$$

The spectroscopy of the formyl radical is also known, in particular the $A\ ^2A'' \leftarrow X\ ^2A'$ absorption band, which spans the visible spectral range and which was first assigned in 1955 by Herzberg and Ramsay [20]. The absorption cross-sections of several rotational transitions near 614 nm have been measured, with peak values of around $4 \cdot 10^{-18} cm^2$ [6].

The experimental results of vinyl radical oxidation studies obtained by TR-BB-CEAS are presented in figures 7 – 10. A 266-nm laser pulse produced C_2H_3 radicals by photolysis of a dilute mixture of 0.9% vinyl iodide [21] in 10 Torr N_2 bath gas. Using photolysis laser fluence of 18 mJ/cm^2, the initial vinyl radical concentration was $1 \cdot 10^{13} cm^{-3}$. An additional variable flow of O_2 was introduced into the reactor, and the oxygen concentration was varied in order to explore its effect on the vinyl radical kinetics.

The left panel in Figure 7 is the transient absorption image of vinyl radical oxidation in the presence of $9 \cdot 10^{14} cm^{-3}$ of oxygen, averaged over 1800 laser shots. The false color scale indicates the transient optical density as a function of kinetic time for the 390 – 705 nm wavelength range. Dominating the image is a strong transient depletion (negative OD), peaked around λ = 500 nm. This negative-going transient is very broad and affects the observed signals at virtually all wavelengths we probe. Yet, because we image the entire transient spectrum at once, we can compare its shape to known gas-phase molecular spectra and easily identify its source. The depletion is due to photodissociation and reactive removal of I_2, which is present in small concentrations as a contaminant in the vinyl iodide sample. By measuring the I_2 transient at 525 nm (where no other species absorb) we can subtract its contribution from the entire image. The resulting image appears in the right panel in Figure 7.

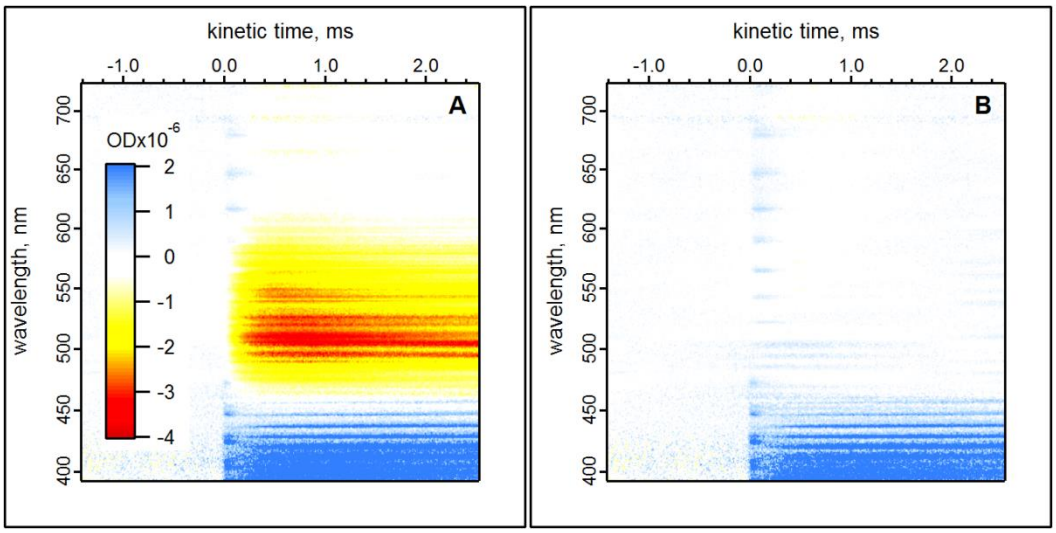

Figure 7. TR-BB-CEAS probing of vinyl oxidation kinetics.
Panel A: Transient OD as a function of probe wavelength and kinetic time. The false color scale denotes the absorption strength. The background signal at negative times (prior to photolysis pulse) has been subtracted. *Panel B*: The same image as the left panel, except that the transient depletion due to I_2 contaminant has been removed.

After the removal of I_2 contribution, three spectral features are apparent in the TR-BB-CEAS image of vinyl radical oxidation kinetics. These features are presented in Figure 8 as transient spectra, averaged over four different kinetic time intervals. The early-time spectrum (0 – 0.1 ms) shows two vibrational progressions, easily assigned to the vinyl [16] and formyl [20] radicals. The vinyl absorption is nearly gone in the 0.1 – 0.2 ms spectrum, while HCO absorption persists, indicating a slower decay than that of the vinyl radical. At around 2 ms both vinyl and formyl signals are absent, replaced by the vibrational progression of IO radicals [22, 23], which are formed by the reaction I + O_2. The IO absorption overlaps with the vinyl radical spectrum, which would ordinarily make measurements of the vinyl kinetics quite difficult. However, the TR-BB-CEAS technique enables a clean deconvolution of vinyl radical decay from IO formation.

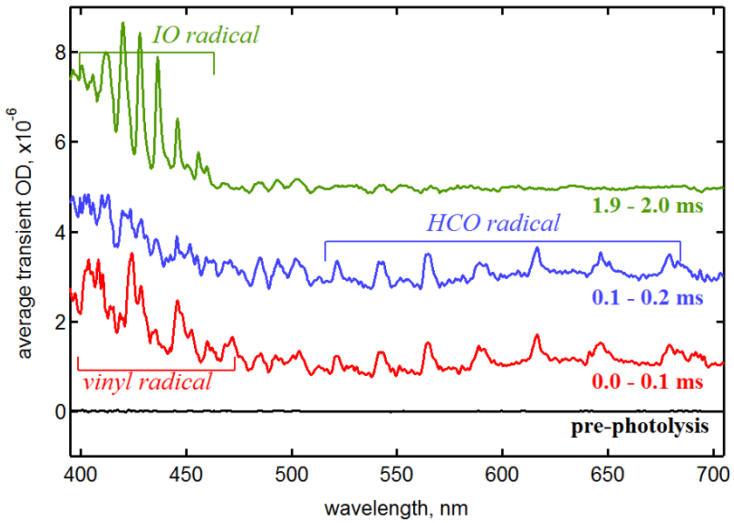

Figure 8. Transient absorption spectra of vinyl radical oxidation

Figure 9 shows kinetic traces for the vinyl radical at several oxygen concentrations. The traces are scaled to match at their maxima for comparison of the decay times. The peak absorption value in the absence of oxygen is OD = $4 \cdot 10^{-6}$ at λ = 404 nm and $2 \cdot 10^{-6}$ at λ = 446 nm, corresponding to an initial concentration of $[C_2H_3] = 6 - 12 \cdot 10^{12}$ cm^{-3}. The range of possible initial concentration values reflects the uncertainty in published vinyl absorption cross-sections [15-17], and overall the agreement with expected initial radical concentration is excellent.

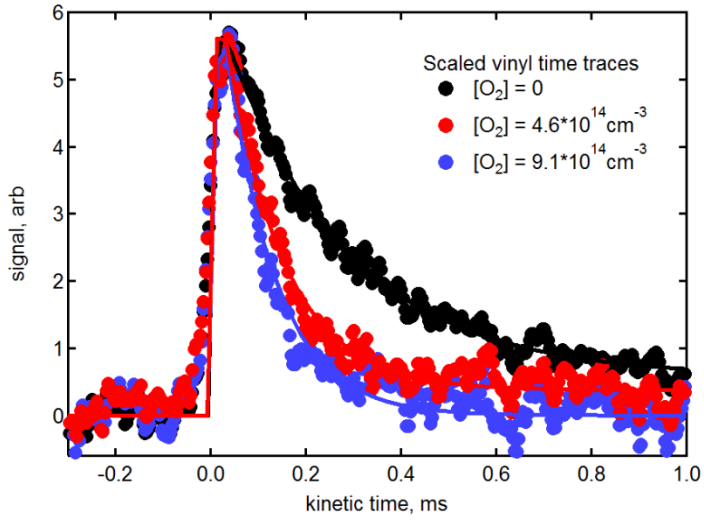

Figure 9. Vinyl radical transients at three different oxygen concentrations.

Figure 10 presents the time traces for HCO, which is produced by reaction $C_2H_3 + O_2$; therefore, HCO rise times are linked with vinyl radical decays. The solid lines in Figures 9 and 10 are fits to experimental data assuming pseudo-first order kinetics. Both figures yield a bimolecular rate coefficient for reaction (2) $k_2 = (10 \pm 1) \cdot 10^{-12}$ $cm^3molec^{-1}s^{-1}$, confirming the literature value [18, 24]. The rate coefficient for reaction (3), extracted from HCO decays, is $k_3 = (3.8 \pm 0.6) \cdot 10^{-12}$ $cm^3molec^{-1}s^{-1}$, in fair agreement with the literature value of $5 \cdot 10^{-12}$ $cm^3molec^{-1}s^{-1}$ [19].

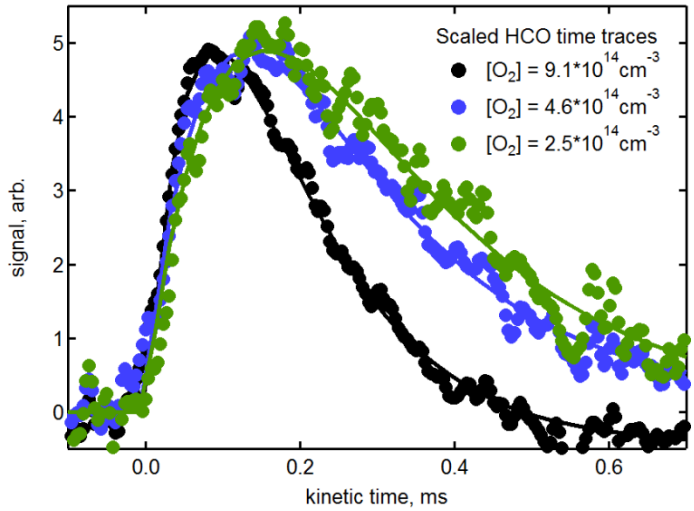

Figure 10. Formyl radical transients as a function of oxygen concentration

5. CONCLUSIONS

We have developed a new method for experimental studies of gas-phase chemical kinetics, time-resolved broadband cavity-enhanced absorption spectroscopy (TR-BB-CEAS). This technique allows simultaneous measurements of transient absorption spectra over the entire visible (370 – 700 nm) spectral range, with μs – level time resolution. Effective path length enhancement is a factor of ~100. Precise determination of absolute concentrations is possible for species with known absorption cross-sections. Probe sensitivity of ~10^{10} – 10^{12} cm^{-3} is possible for strong to moderately strong molecular absorbers, which represents approximately two orders of magnitude improvement over conventional spectroscopy approaches. Detection efficiency can be enhanced further by simple modifications to the experimental setup, most notably the optics in the spectrometer design.

The power of TR-BB-CEAS was demonstrated by the detection and experimental investigation of short-lived reaction intermediates: the vinyl and formyl radicals. An extension of the new method to the near-UV spectral range (300 – 400 nm) is already underway, which will greatly increase the accessible pool of experimental targets and make this a widely applicable experimental tool.

6. REFERENCES

1. Ball, S.M. and R.L. Jones, *Broad-band cavity ring-down spectroscopy.* Chemical Reviews, 2003. **103**(12): p. 5239-5262.
2. Brown, S.S., *Absorption spectroscopy in high-finesse cavities for atmospheric studies.* Chemical Reviews, 2003. **103**(12): p. 5219-5238.
3. Engeln, R., et al., *Cavity enhanced absorption and cavity enhanced magnetic rotation spectroscopy.* Review of Scientific Instruments, 1998. **69**(11): p. 3763-3769.
4. Zalicki, P. and R.N. Zare, *Cavity Ring-down Spectroscopy for Quantitative Absorption-Measurements.* Journal of Chemical Physics, 1995. **102**(7): p. 2708-2717.
5. Siegman, A.E., *Lasers*1986, Mill Valley, CA: University Science Books.
6. Flad, J.E., et al., *Absorption cross sections for the (A)over-tilde(2)A ''(0,9(0),0)<-(X)over-tilde(2)A '(0,0(1),0) band of the HCO radical.* Physical Chemistry Chemical Physics, 2006. **8**(31): p. 3636-3642.
7. Miller, T.A., *Spectroscopic probing and diagnostics of the geometric structure of the alkoxy and alkyl peroxy radical intermediates.* Molecular Physics, 2006. **104**(16-17): p. 2581-2593.
8. Paldus, B.A., et al., *Cavity-locked ring-down spectroscopy.* Journal of Applied Physics, 1998. **83**(8): p. 3991-3997.
9. Spence, T.G., et al., *A laser-locked cavity ring-down spectrometer employing an analog detection scheme.* Review of Scientific Instruments, 2000. **71**(2): p. 347-353.
10. Fiedler, S.E., A. Hese, and A.A. Ruth, *Incoherent broad-band cavity-enhanced absorption spectroscopy.* Chemical Physics Letters, 2003. **371**(3-4): p. 284-294.
11. Scherer, J.J., et al., *Broadband ringdown spectral photography.* Applied Optics, 2001. **40**(36): p. 6725-6732.
12. Bogumil, K., et al., *Measurements of molecular absorption spectra with the SCIAMACHY pre-flight model: instrument characterization and reference data for atmospheric remote-sensing in the 230-2380 nm region.* Journal of Photochemistry and Photobiology a-Chemistry, 2003. **157**(2-3): p. 167-184.
13. Carbajo, P.G. and A.J. Orr-Ewing, *NO2 quantum yields from ultraviolet photodissociation of methyl and isopropyl nitrate.* Physical Chemistry Chemical Physics, 2010. **12**(23): p. 6084-6091.
14. Laufer, A.H. and A. Fahr, *Reactions and kinetics of unsaturated C-2 hydrocarbon radicals.* Chemical Reviews, 2004. **104**(6): p. 2813-2832.
15. DeSain, J.D., L.E. Jusinski, and C.A. Taatjes, *Ultraviolet photochemistry of trichlorovinylsilane and allyltrichlorosilane: vinyl radical (HCCH2) and allyl radical (H2CCHCH2) production in 193 nm photolysis.* Physical Chemistry Chemical Physics, 2006. **8**(19): p. 2240-2248.
16. Shahu, M., et al., *Vinyl radical visible spectroscopy and excited state dynamics.* Journal of Chemical Physics, 2002. **116**(19): p. 8343-8352.
17. Tonokura, K., S. Marui, and M. Koshi, *Absorption cross-section measurements of the vinyl radical in the 440-460 nm region by cavity ring-down spectroscopy.* Chemical Physics Letters, 1999. **313**(5-6): p. 771-776.

18. Eskola, A.J. and R.S. Timonen, *Kinetics of the reactions of vinyl radicals with molecular oxygen and chlorine at temperatures 200-362 K.* Physical Chemistry Chemical Physics, 2003. **5**(12): p. 2557-2561.
19. Baulch, D.L., et al., *Evaluated Kinetic Data for Combustion Modeling.* Journal of Physical and Chemical Reference Data, 1992. **21**(3): p. 411-734.
20. Herzberg, G. and D.A. Ramsay, *The 7500 to 4500 a Absorption System of the Free Hco Radical.* Proceedings of the Royal Society of London Series a-Mathematical and Physical Sciences, 1955. **233**(1192): p. 34-54.
21. Zou, P., et al., *Ultraviolet photodissociation of vinyl iodide: understanding the halogen dependence of photodissociation mechanisms in vinyl halides.* Physical Chemistry Chemical Physics, 2008. **10**(5): p. 713-728.
22. Bloss, W.J., et al., *Kinetics of the ClO self-reaction and 210 nm absorption cross section of the ClO dimer.* Journal of Physical Chemistry A, 2001. **105**(50): p. 11226-11239.
23. Harwood, M.H., et al., *Absorption cross sections and self-reaction kinetics of the IO radical.* Journal of Physical Chemistry A, 1997. **101**(5): p. 853-863.
24. Knyazev, V.D. and I.R. Slagle, *Kinetics of the Reaction of Vinyl Radical with Molecular-Oxygen.* Journal of Physical Chemistry, 1995. **99**(8): p. 2247-2249.

DISTRIBUTION

1	MS0899	Technical Library	9536 (electronic copy)
1	MS0359	D. Chavez, LDRD Office	1911


Sandia National Laboratories